Journal of Innovations in Engineering Education
JIEE 2025, Vol. 8, Issue 1.

https://doi.org/10.3126/jiee.v8i1.77044

THAPATHALI CAMPUS
Institute of Engineering
Tribhuvan University

Forced vibration of multidisc Shaft with rotating unbalance

Bishwas Gautam[a,*], Mahesh Chandra Luitel [b] and Pankaj Yadav [c]

[a] *Institute of Engineering, Thapathali Campus, Thapathali*
[b] *Institute of Engineering, Pulchowk Campus, Lalitpur*
[c] *Institute of Engineering, Pashchimanchal Campus, Lamachaur*

ARTICLE INFO

Article history:

Received 25 March 2025
Revised in 29 March 2025
Accepted 1 April 2025

Keywords:

Euler-Bernoulli beam
Gyroscopic effect
Extended Hamilton's principle
Unbalance
Amplitude

Abstract

Most of the modern day engineering systems use rotor dynamics for the transmission of power. The slightest imbalance in the rotor system can create a massive loss in the energy transfer and the system's life. This study explores the dynamic behavior of multidisc shaft systems with rotating unbalance, a crucial area in mechanical engineering, by integrating analytical modeling, mathematical formulations, and finite element simulations using ANSYS. The shaft is modeled as a flexible Euler-Bernoulli beam, considering the gyroscopic effect, while the discs are considered rigid bodies with unbalance present in a disc. The equations of motion are derived using Extended Hamilton's principle and solved to evaluate the system's forced vibration response. For the system considered, which is rotating at the speed of 1500 RPM, in both transverse directions, the amplitude at the end of the shaft was found to be 41.495 micrometers, considering the unbalance of 0.0001kgm present at first disc positioned at one-third length of the shaft. The amplitude was 18.46 micrometers at the position of the second disc situated at two-thirds length of the shaft. The analytical results were considered with the numerical results of ANSYS, and variation in result was found to be less than 10 percent.

1. Introduction

Rotors and rotating parts are foundational in engineering applications like pumps, compressors, turbines, and generators, where their dynamic behavior directly impacts operational efficiency and structural integrity [1]. The transmission of power is the main motive for the use of the disc and shaft systems. Rotating machinery must be closely monitored to detect faults, which may arise due to operating conditions or manufacturing defects. Rotating unbalance occurs when mass is unevenly distributed around the rotational axis. A rotor is considered unbalanced when its inertial axis, or center of mass, does not align with its geometric axis. This misalignment creates a moment, causing the rotor to wobble. The combination of mass unbalance and radial acceleration due to rotation generates centrifugal forces, which increase bearing loads and induce vibrations within the system [2].

*Corresponding author:
bishwasg135@gmail.com (B. Gautam)

The field of vibration analysis on a shaft rotor system is still under research. Different researchers have contributed to this field. Geradin et al [3] analyzed a three-dimensional modelling of the rotating system for the calculation of critical speed and analyzing its stability. Shaw et.al [4] studied the dynamic response of an unbalanced rotating shaft. They investigated the steady state solution for the synchronous rotation of the shaft. Hosseini et. al [5] found the natural frequency of a simply supported rotating shaft with non-linearity, including the effect of rotary inertia and gyroscopic. The equation of motion was derived using Hamilton's principle and the resonance curve. Luintel et.al [6] focused on the dynamic response of continuous shafts with various end conditions. The equation of motion for the bending vibration of the shaft was derived using Hamilton's principle. The assumed mode method was applied to obtain the governing equation for both simply supported and fixed-end shafts. Free vibration analysis was conducted to determine the critical frequencies for each case. Also, Luintel et.al [7] formulated the polynomial mode shape

functions for continuous shafts with various end conditions. The equation of motion for the continuous shaft system, considering various end conditions like simply supported, both ends fixed, and one end fixed and the other free, was derived. The assumed mode method was employed to solve the equation of motion, resulting in the calculation of three mode shape functions for all cases.

Furthermore, Ojha et.al [8] studied the behavior of three-disc arrangements: equal mass at equal distances, varying masses at equal distances, and equal mass at different distances. Using an extended form of Hamilton's principle, the equations of motion are derived and transformed into time-domain equations via the assumed mode method. Modal parameters and critical speeds for forward and backward whirl are determined. The analytical results closely match the simulation findings, validating the model's accuracy. Pradhan et.al [9] focused on the modal analysis of a multi-disc rotor system, finding the natural frequency with an analytical approach closely validated by the finite element method.

Ameen et.al [10] studied modal parameters for the free-free boundary condition of a circular cross-section shaft. The parameters natural frequency, mode shape and damping ratios were studied using Experimental Modal Analysis (EMA) and were validated using Finite Element Modelling (FEM). Saleem et.al [11] focused on the Deflected Shape of the Shaft (DSS) of a rotating machine, which was found for determining the unbalance in the machine component. Fast Fourier Transform (FFT) was used for vibration data. Kumar et.al [12] performed experimental studies to find the unbalance in the rotor. By performing the spectrum analysis and phase analysis, the cause of the high vibration was determined. Miranda et.al [13] present an experimental and numerical analysis of the transverse vibration of a fixed-free beam, focusing on mode shapes and frequencies. Numerical results from ANSYS finite element analysis align well with experimental findings. A finite element method for eigenvalue analysis of damped gyroscopic systems, more especially, flexible rotors on fluid film journal bearings, was created in ref. [14] .They examined the impact of effective damping on eigenvalues in rotor-bearing systems and examined natural frequencies under varied operating conditions using the Galerkin weighted residual method on Reynolds' equation.

Existing research on forced vibrations primarily focuses on simpler single-disc shaft systems, neglecting the additional complexities introduced by multiple discs. There is a gap in understanding the response of a multi-disc shaft system subjected to rotating unbalance, which may result from manufacturing defects, eccentricity in design or installation, wear, and material loss. This research aims to fill this gap by developing a comprehensive model to analyze the forced vibrations of multi-disc cantilever shaft systems under rotating unbalance. The goal is to provide insights into the system's dynamic behavior.

The main objective of this research is to study the forced vibration behavior of a multi-disc cantilever shaft system subjected to rotating unbalance. To achieve the main objective, a mathematical model will be formulated for a two-disc shaft system, and the model will be analyzed analytically, evaluating the steady-state response at various positions along the length of the shaft. The model will be validated through ANSYS simulation.

2. Development of Mathematical model

2.1. Mathematical modelling of Disc

The rotor dynamic system consists of two discs and a rotating shaft. The disc is assumed to be rigid. The axis y represents the longitudinal direction of the shaft, x represents the transverse direction in the horizontal plane, and z represents the transverse direction in the vertical plane. The global coordinate system X, Y, Z is fixed, and the rotating frame labeled x, y, z, fixed with the center of the disc, moves with the rotating shaft. The coordinate system is illustrated in Figure 1.

The angular speed vector $[\omega_x,\ \omega_y,\ \omega_z]$ defined about

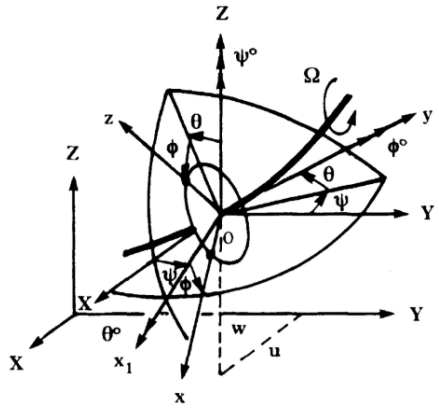

Figure 1: Global Coordinate System and Rotating Frame

the reference frame x, y, z at the center of the disc is given in Ref.[1] as:

$$\begin{bmatrix} \omega_x \\ \omega_y \\ \omega_z \end{bmatrix} = \begin{bmatrix} -\dot{\psi}\,\phi + \dot{\theta} \\ \dot{\phi} + \dot{\psi}\,\theta \\ \dot{\psi} + \dot{\theta}\,\phi \end{bmatrix} \tag{1}$$

Where θ, ϕ, and ψ are the Euler angles.

The displacements of the center of mass of the disc in the X and Z directions of the inertial reference frame are denoted by u and w, respectively. If M_D represents the mass of the disc, then the kinetic energy of the disc is the sum of translational kinetic energy and rotational kinetic energy.

$$T_D = \frac{1}{2} M_D \left(\dot{u}^2 + \dot{w}^2\right) + \frac{1}{2}\left(I_{DX}\omega_X^2 + I_{DY}\omega_Y^2 + I_{DZ}\omega_Z^2\right) \tag{2}$$

Where I_{DX}, I_{DY}, and I_{DZ} are the mass moments of inertia of the disc about x, y, and z, respectively.

The disc is rotated about the y-axis with constant rotational speed Ω. Then, $\dot{\phi} = \Omega$ (rate of spin, constant), and θ and ψ are very small.

Then Equation 2 becomes

$$T_D = \frac{1}{2} M_D \left(\dot{u}^2 + \dot{w}^2\right) \frac{1}{2} I_{DX}\left(\dot{\theta}^2 + \dot{\psi}^2\right) + \frac{1}{2} I_{DY}\left(\Omega^2 + 2\Omega\,\dot{\psi}\,\theta\right) \tag{3}$$

Where $I_{DY}\,\Omega\,\dot{\psi}\,\theta$ accounts for the gyroscopic effect.

2.2. Mathematical modelling of Shaft

The shaft is assumed to be a beam with a constant circular cross section and is characterized by strain and kinetic energy. Figure 2 illustrates the shaft's cross-section along with two reference frames: the inertial frame, where displacements are measured as u and w along the X and Z axes, and the rotating frame concerning the center of the cross-section of the shaft along the x and z axes.

The kinetic energy of the shaft, represented by T_s, is:

$$T_s = \frac{1}{2}\rho_s A_s \int_0^L \left(\dot{u}^2 + \dot{w}^2\right) dy + \frac{1}{2}\rho_s I_s \int_0^L \left(\dot{\theta}^2 + \dot{\psi}^2\right) dy + \rho_s I_s L\,\Omega^2 + 2\rho_s I_s \Omega \int_0^L \dot{\psi}\,\theta\, dy \tag{4}$$

Where ρ_s, I_s, and A_s denote the density, mass moment of inertia, and cross-sectional area of the shaft, respectively.

The strain energy of the shaft due to bending is given by:

$$V_s = \frac{1}{2} E I_{zz} \int_0^L \left[\left(u''\right)^2 + \left(w''\right)^2\right] dy \tag{5}$$

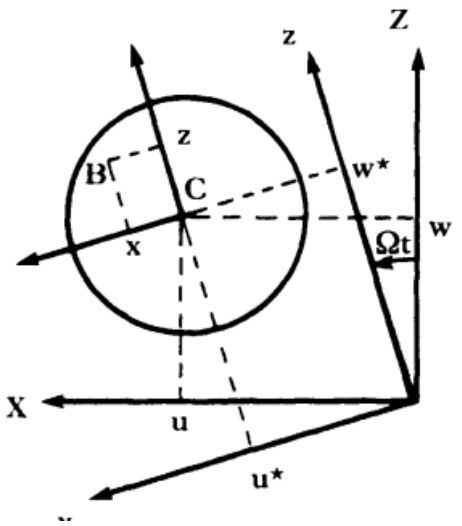

Figure 2: Cross-section of shaft with two frames

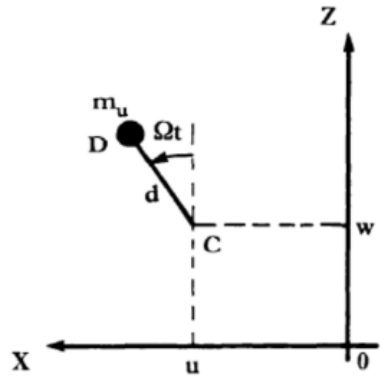

Figure 3: Rotating Unbalance taken as point mass (m_u)

2.3. Rotating unbalance in Disc

The mass unbalance is represented as a point mass (m_u) positioned at a distance d from the shaft's center.

As the unbalance point mass (m_u) is much smaller than the disc's mass. The expression for the kinetic energy of unbalanced mass, which acts as a non-conservative force, is given by:

$$W_{nc} = m_u\,\Omega e\left(\dot{u}\cos\Omega t + \dot{w}\sin\Omega t\right) \tag{6}$$

2.4. Problem formulation

A model for two-discs mounted on a shaft used to study forced vibrations due to rotating unbalance. The system consists of two rigid discs: the first disc is present at one-third of the length of the shaft, and the second disc is present at two-thirds of the length of the shaft, as shown in Figure 4. The rotating unbalance is present in the first disc.

The total kinetic energy for the system is given by:

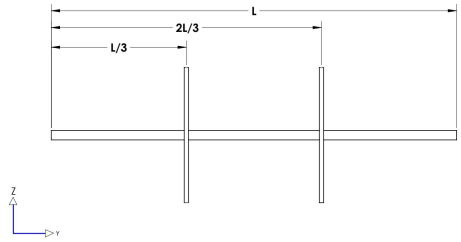

Figure 4: A wireframe modelling of the shaft-disc system

$$
\begin{aligned}
T &= T_{1D} + T_{2D} + T_S \\
&= \frac{1}{2} M_{1D} \int_0^L \left(\dot{u}^2 + \dot{w}^2\right) \delta_d \left(y - \frac{L}{3}\right) dy + \\
&\quad \frac{1}{2} I_{1DX} \int_0^L \left(\dot{\theta}^2 + \dot{\psi}^2\right) \delta_d \left(y - \frac{L}{3}\right) dy + \\
&\quad \frac{1}{2} I_{1DY} \int_0^L \left(\Omega^2 + 2\Omega\dot{\psi}\theta\right) \delta_d \left(y - \frac{L}{3}\right) dy \\
&\quad + \frac{1}{2} M_{2D} \int_0^L \left(\dot{u}^2 + \dot{w}^2\right) \delta_d \left(y - \frac{2L}{3}\right) dy + \\
&\quad \frac{1}{2} I_{2DX} \int_0^L \left(\dot{\theta}^2 + \dot{\psi}^2\right) \delta_d \left(y - \frac{2L}{3}\right) dy \\
&\quad + \frac{1}{2} I_{2DY} \int_0^L \left(\Omega^2 + 2\Omega\dot{\psi}\theta\right) \delta_d \left(y - \frac{2L}{3}\right) dy \\
&\quad + \frac{1}{2} \rho_s A_s \int_0^L \left(\dot{u}^2 + \dot{w}^2\right) dy + \frac{1}{2} \rho_s I_s \int_0^L \left(\dot{\theta}^2 + \dot{\psi}^2\right) \\
&\quad dy + \rho_s I_s L\, \Omega^2 + 2\rho_s I_s \Omega \int_0^L \dot{\psi}\, \theta\, dy
\end{aligned}
\tag{7}
$$

The total potential energy for the shaft is given by Equation 5.

2.5. Equation of motion

The equation of motion for the model is found using the Extended Hamilton principle.

Using the Extended Hamilton principle,

$$
\int_{t_1}^{t_2} \left(T - V + W_{nc}\right) dt = 0 \tag{8}
$$

$$
\begin{aligned}
&\frac{1}{2} M_{1D} \int_{t_1}^{t_2} \int_0^L \delta \left(\dot{u}^2 + \dot{w}^2\right) \delta_d \left(y - \frac{L}{3}\right) dy\, dt \\
&\quad + \frac{1}{2} I_{1DX} \int_{t_1}^{t_2} \int_0^L \delta \left(\dot{\theta}^2 + \dot{\psi}^2\right) \delta_d \left(y - \frac{L}{3}\right) dy\, dt \\
&\quad + \frac{1}{2} I_{1DY} \int_{t_1}^{t_2} \int_0^L \delta \left(\Omega^2 + 2\Omega\dot{\psi}\theta\right) \delta_d \left(y - \frac{L}{3}\right) dy\, dt \\
&\quad + \frac{1}{2} M_{2D} \int_{t_1}^{t_2} \int_0^L \delta \left(\dot{u}^2 + \dot{w}^2\right) \delta_d \left(y - \frac{2L}{3}\right) dy\, dt \\
&\quad + \frac{1}{2} I_{2DX} \int_{t_1}^{t_2} \int_0^L \delta \left(\dot{\theta}^2 + \dot{\psi}^2\right) \delta_d \left(y - \frac{2L}{3}\right) dy\, dt \\
&\quad + \frac{1}{2} I_{2DY} \int_{t_1}^{t_2} \int_0^L \delta \left(\Omega^2 + 2\Omega\dot{\psi}\theta\right) \delta_d \left(y - \frac{2L}{3}\right) dy\, dt \\
&\quad + \frac{1}{2} \rho_s A_s \int_{t_1}^{t_2} \int_0^L \delta \left(\dot{u}^2 + \dot{w}^2\right) dy\, dt \\
&\quad + \frac{1}{2} \rho_s I_s \int_{t_1}^{t_2} \int_0^L \delta \left(\dot{\theta}^2 + \dot{\psi}^2\right) dy\, dt \\
&\quad + \rho_s I_s L\, \Omega^2 + 2\rho_s I_s \Omega \int_{t_1}^{t_2} \int_0^L \delta \left(\dot{\psi}\, \theta\right) dy\, dt \\
&\quad - \frac{1}{2} E I_{zz} \int_{t_1}^{t_2} \int_0^L \left[\left(u''\right)^2 + \left(w''\right)^2\right] dy\, dt \\
&\quad + m_u\, \Omega e \int_{t_1}^{t_2} \int_0^L \delta \left(\dot{u} \cos \Omega t + \dot{w} \sin \Omega t\right) \delta_d \left(y - \frac{L}{3}\right) \\
&\quad dy\, dt = 0
\end{aligned}
\tag{9}
$$

On Solving we get equation of motion as:

$$
\begin{aligned}
&M_{1D}\, \ddot{u}\, \delta_d \left(y - \frac{L}{3}\right) + M_{2D}\, \ddot{u}\, \delta_d \left(y - \frac{2L}{3}\right) \\
&\quad - I_{1DX}\, u''\, \delta w\, \delta_d \left(y - \frac{L}{3}\right) - I_{2DX}\, u''\, \delta w\, \delta_d \left(y - \frac{2L}{3}\right) \\
&\quad - I_{1DY}\, w''\, \delta_d \left(y - \frac{L}{3}\right) - I_{2DY}\, w''\, \delta_d \left(y - \frac{2L}{3}\right) \\
&\quad + \rho_s A_s\, \ddot{u} - \rho_s I_s\, u'' - 2\rho_s I_s\, \Omega\, w'' + E I_{zz}\, u^{\mathrm{iv}} \\
&= m_u\, \Omega^2\, e\, \sin \Omega t\, \delta_d \left(y - \frac{L}{3}\right)
\end{aligned}
\tag{10}
$$

$$
\begin{aligned}
&M_{1D}\, \ddot{w}\, \delta_d \left(y - \frac{L}{3}\right) + M_{2D}\, \ddot{w}\, \delta_d \left(y - \frac{2L}{3}\right) \\
&\quad - I_{1DX}\, w''\, \delta_d \left(y - \frac{L}{3}\right) - I_{2DX}\, w''\, \delta_d \left(y - \frac{2L}{3}\right) \\
&\quad + I_{1DY}\, \Omega\, u''\, \delta_d \left(y - \frac{L}{3}\right) + I_{2DY}\, u''\, \delta_d \left(y - \frac{2L}{3}\right) \\
&\quad + \rho_s A_s\, \ddot{w} - \rho_s I_s\, w'' + 2\rho_s I_s\, \Omega\, u'' + E I_{zz}\, w^{\mathrm{iv}} \\
&= m_u\, \Omega^2\, e\, \cos \Omega t\, \delta_d \left(y - \frac{L}{3}\right)
\end{aligned}
\tag{11}
$$

3. Results

3.1. Separation of variables

For solving the equations of motion defined by equations 10 and 11, the separation of variables method was used. The solution to the given equations was assumed to be the product of two independent functions: one space-dependent, $\psi_i(y)$, and the other time-dependent, $q_i(t)$. The transverse displacement in the horizontal plane is assumed to be given by equation 12, and in the vertical plane is given by equation 13.

$$u_i(y,t) = \psi_i(y)\, q_{iu}(t) \tag{12}$$

$$w_i(y,t) = \psi_i(y)\, q_{iw}(t) \tag{13}$$

3.2. Shape function

A shape function defines the displacements of a structure in terms of spatial coordinates. This function defines the mode shape and helps us find the natural frequency as well as the dynamic response. These functions are derived from the boundary condition of the system. The formulation ensures that displacement and slope continuity are maintained, providing an accurate representation of the beam's deformation behavior. The first three mode shapes for the cantilever beam taken from ref. [15] as:

$$\psi_1(y) = y^4 - 4Ly^3 + 6L^2y^2 \tag{14}$$

$$\psi_2(y) = y^5 - \frac{661}{182}Ly^4 + \frac{412}{91}L^2y^3 - \frac{163}{91}L^3y^2 \tag{15}$$

$$\psi_3(y) = y^6 - \frac{9953}{2608}Ly^5 + \frac{305815}{57376}L^2y^4 - \frac{5560}{1793}L^3y^3 + \frac{115}{176}L^4y^2 \tag{16}$$

3.3. Galerkin method

The Galerkin method is a technique used to convert continuous problems governed by differential equations into discrete problems for easier solutions. The Galerkin method approximates the solution by expanding it in terms of basis functions, typically chosen to satisfy the problem's boundary conditions. The method minimizes the residual (error) between the exact and approximate solutions by selecting test functions equal to the basis functions. This leads to a system of algebraic equations that can be solved to find the unknown coefficients.

For solving the equation of motion, the Galerkin method is used. The residual required for solving the equation using the Galerkin method are:

$$\begin{aligned} R_1 = {} & M_{1D}\,\ddot{u}\,\delta_d\left(y-\frac{L}{3}\right) + M_{2D}\,\ddot{u}\,\delta_d\left(y-\frac{2L}{3}\right) \\ & - I_{1DX}\,u''\,\delta w\,\delta_d\left(y-\frac{L}{3}\right) \\ & - I_{2DX}\,u''\,\delta w\,\delta_d\left(y-\frac{2L}{3}\right) \\ & - I_{1DY}\,w''\,\delta_d\left(y-\frac{L}{3}\right) - I_{2DY}\,w''\,\delta_d\left(y-\frac{2L}{3}\right) \\ & + \rho_s A_s\,\ddot{u} - \rho_s I_s\,u'' + 2\rho_s I_s\,\Omega\,w'' + EI_{zz}\,u^{\mathrm{iv}} \\ & - m_u\,\Omega^2\,e\,\sin\Omega t\,\delta_d\left(y-\frac{L}{3}\right) \end{aligned} \tag{17}$$

$$\begin{aligned} R_2 = {} & M_{1D}\,\ddot{w}\,\delta_d\left(y-\frac{L}{3}\right) + M_{2D}\,\ddot{w}\,\delta_d\left(y-\frac{2L}{3}\right) \\ & - I_{1DX}\,w''\,\delta_d\left(y-\frac{L}{3}\right) - I_{2DX}\,w''\,\delta_d\left(y-\frac{2L}{3}\right) \\ & - I_{1DY}\,\Omega\,u''\,\delta_d\left(y-\frac{L}{3}\right) - I_{2DY}\,u''\,\delta_d\left(y-\frac{2L}{3}\right) \\ & + \rho_s A_s\,\ddot{w} - \rho_s I_s\,w'' - 2\rho_s I_s\,\Omega\,u'' + EI_{zz}\,w^{\mathrm{iv}} \\ & - m_u\,\Omega^2\,e\,\cos\Omega t\,\delta_d\left(y-\frac{L}{3}\right) \end{aligned} \tag{18}$$

Using the Galerkin Method,

$$\int_0^L \psi_i(y)\,R_1\,dy = 0 \tag{19}$$

Putting equations 14 and 17 in equation 19, we get,

$$\begin{aligned} & \left[M_{1D}\,\psi_i^2\Big|_{y=L/3} + M_{2D}\,\psi_i^2\Big|_{y=2L/3} - I_{1DX}\,\psi_i''\,\psi_i\Big|_{y=L/3}\right. \\ & - I_{2DX}\,\psi_i''\,\psi_i\Big|_{y=2L/3} + \rho_s A_s\int_0^L \psi_i^2\,dy \\ & \left. - \rho_s I_s\int_0^L \psi_i''\,\psi_i\,dy\right]\ddot{q}_{1U} - \left[I_{1DY}\,\Omega\,\psi_i''\,\psi_i\Big|_{y=L/3}\right. \\ & \left. + I_{2DY}\,\Omega\,\psi_i''\,\psi_i\Big|_{y=2L/3} + 2\rho_s I_s\,\Omega\int_0^L \psi_i''\,\psi_i\,dy\right]\dot{q}_{1W} \\ & + \left[EI_{zz}\int_0^L \psi_i''''\,\psi_i\,dy\right]q_{1U} \\ & = m_u\,\Omega^2\,e\,\sin\Omega t\,\psi_i\Big|_{y=L/3} \end{aligned} \tag{20}$$

$$\int_0^L \psi_i(y)\,R_2\,dy = 0 \tag{21}$$

Putting equations 14 and 18 in equation 21, we get,

$$\begin{aligned}&\left[M_{1D}\,\psi_i^2\Big|_{y=L/3}+M_{2D}\,\psi_i^2\Big|_{y=2L/3}-I_{1DX}\,\psi_i''\,\psi_i\Big|_{y=L/3}\right.\\&-I_{2DX}\,\psi_i''\,\psi_i\Big|_{y=2L/3}+\rho_s A_s\int_0^L\psi_i^2\,dy\\&\left.-\rho_s I_s\int_0^L\psi_i''\,\psi_i\,dy\right]\ddot{q}_{1U}+\left[I_{1DY}\,\Omega\,\psi_i''\,\psi_i\Big|_{y=L/3}\right.\\&\left.+I_{2DY}\,\Omega\,\psi_i''\,\psi_i\Big|_{y=2L/3}+2\rho_s I_s\,\Omega\int_0^L\psi_i''\,\psi_i\,dy\right]\dot{q}_{1W}\\&+\left[EI_{ZZ}\int_0^L\psi_i''''\,\psi_i\,dy\right]q_{1U}\\&=m_u\,\Omega^2\,e\,\cos\Omega t\,\psi_i\Big|_{y=L/3}\end{aligned}\tag{22}$$

Comparing equation 20 with equation 23, we have:

$$M_i\,\ddot{q}_{1U}-C_i\,\dot{q}_{1W}+K_i\,q_{1U}=F_i\,\sin\Omega t\tag{23}$$

Comparing equation 22 with equation 24, we have:

$$M_i\,\ddot{q}_{1W}+C_i\,\dot{q}_{1U}+K_i\,q_{1W}=F_i\,\cos\Omega t\tag{24}$$

We get,

$$\begin{aligned}M_i=&M_{1D}\,\psi_i^2\Big|_{y=L/3}+M_{2D}\,\psi_i^2\Big|_{y=2L/3}\\&-I_{1DX}\,\psi_i''\,\psi_i\Big|_{y=L/3}-I_{2DX}\,\psi_i''\,\psi_i\Big|_{y=2L/3}\\&+\rho_s A_s\int_0^L\psi_i^2\,dy-\rho_s I_s\int_0^L\psi_i''\,\psi_i\,dy\end{aligned}\tag{25}$$

$$\begin{aligned}C_i=&I_{1DY}\,\Omega\,\psi_i''\,\psi_i\Big|_{y=L/3}+I_{2DY}\,\Omega\,\psi_i''\,\psi_i\Big|_{y=2L/3}\\&+2\rho_s I_s\,\Omega\int_0^L\psi_i''\,\psi_i\,dy\end{aligned}\tag{26}$$

$$K_i=EI_{ZZ}\int_0^L\psi_i''''\,\psi_i\,dy\tag{27}$$

$$F_i=m_U\,\Omega^2\,e\,\psi_1\Big|_{y=L/3}\tag{28}$$

3.4. Steady state solution of temporal equation

For solving equations 23 and 24, the solution can be sought in the form of:

$$q_{iu}=A_i\,\sin\Omega t+B_i\,\cos\Omega t\tag{29}$$

$$q_{iw}=C_i\,\sin\Omega t+D_i\,\cos\Omega t\tag{30}$$

Putting equations 29 and 30 into 23 and 24, we have the following values:

$$B_i=0$$

$$C_i=0$$

$$A_i=\frac{F_i}{K_i-\Omega^2M_i+\Omega C_i}\tag{31}$$

$$D_i=\frac{F_i}{K_i-\Omega^2M_i+\Omega C_i}\tag{32}$$

Substituting these values into equations 29 and 30, we get the solution as:

$$q_{iu}=\frac{F_i}{K_i-\Omega^2M_i+\Omega C_i}\,\sin\Omega t\tag{33}$$

$$q_{iw}=\frac{F_i}{K_i-\Omega^2M_i+\Omega C_i}\,\cos\Omega t\tag{34}$$

The transverse displacements are found to be:

$$\begin{aligned}u_i(y,t)&=\psi_i(y)\,q_{iu}(t)\\&=\psi_i(y)\,\frac{F_i}{K_i-\Omega^2M_i+\Omega C_i}\,\sin\Omega t\end{aligned}\tag{35}$$

$$\begin{aligned}w_i(y,t)&=\psi_i(y)\,q_{iw}(t)\\&=\psi_i(y)\,\frac{F_i}{K_i-\Omega^2M_i+\Omega C_i}\,\cos\Omega t\end{aligned}\tag{36}$$

4. Results and discussion

The results for the proposed model are found using the basic parameters given in Table 1.

4.1. Analytical results

4.1.1. Modal Mass, Damping, and Stiffness

Using the above parameters in equation 23, 24, 25, and 26 we get modal mass, damping and stiffness for the first three modes of vibrations as shown in Table 2.

Table 1: Basic System Parameters

System Parameters	Value
Shaft length (L_s)	0.6 m
Shaft Diameter (D_s)	0.014 m
Disc Outer Diameter (D_o)	0.2 m
Density of shaft (ρ_d)	7680 kg/m^3
Mass of Disc (M_D)	1.5 kg
Density of shaft (ρ_s)	7680 kg/m^3
Modulus of Elasticity (E)	207×10^9 N/m^2
Unbalanced mass (m_u)	0.01 kg
Eccentricity (e)	0.01 m
Rotational velocity (Ω)	157.08 rad/s

Table 2: Modal Parameters of the System

Mode	Mass (kg)	Damping (N.s/m)	Stiffness (N/m)	Force (N)
First	0.104766545	0.280256323	874.180065	0.16975799
Second	8.41847E-05	-0.00283514	17.48043436	-0.013826187
Third	0.000001254002321	2.80716E-05	0.614539851	0.00106145

4.1.2. *Displacement function at different positions of Shaft in horizontal plane*

The transverse displacement $u(y,t)$ at different positions is given by equation 35. Using equations 15, 16, 17, 26, 27, 28, and 29 in equation 35, we get the displacements as shown in Table 3.

The graphical representation of transverse displacement in the Horizontal plane at various shaft positions is shown in Figure 5.

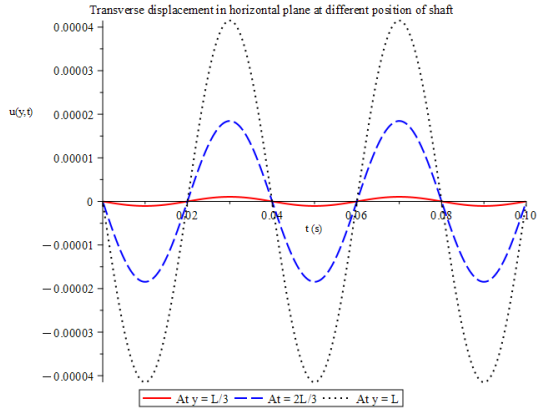

Figure 5: Transverse displacement in horizontal plane at different position of shaft at the rotating speed of 1500 RPM

4.1.3. *Displacement function at different positions of Shaft in vertical plane*

The transverse displacement $w(y,t)$ at different positions is given by equation 36. Using equations 15, 16, 17, 26, 27, 28, and 29 in equation 36, we get the displacement shown in Table 4. The graphical representation of transverse displacement in the Vertical plane at various shaft positions is shown in Figure 6.

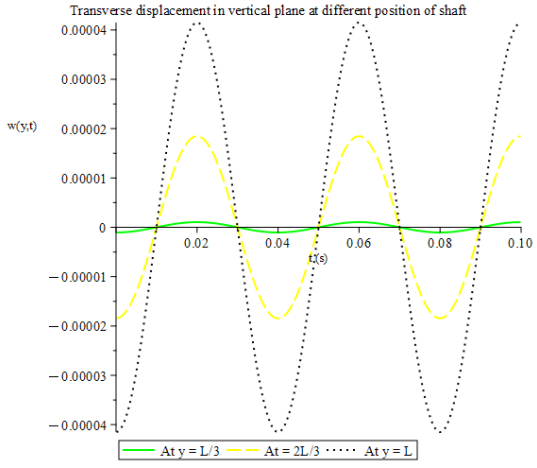

Figure 6: Transverse displacement in the vertical plane at different positions of the shaft at the rotating speed of 1500 RPM

4.2. Harmonic analysis: Validation Using ANSYS

4.2.1. *Geometric model with point mass*

To validate the result obtained from the Analytical results, a model was created on ANSYS Workbench 2024R1 to evaluate the result. The disc was assumed to

Table 3: Transverse displacement $u(y,t)$ at various shaft positions

Mode	**At one-third of the shaft** ($y = L/3$)	**At two-thirds of the shaft** ($y = 2L/3$)	**At the end of the shaft** ($y = L$)
First	$-7.01\ \mu$m $\sin 157.08t$	$-22.62\ \mu$m $\sin 157.08t$	$-39.597\ \mu$m $\sin 157.08t$
Second	$5.18\ \mu$m $\sin 157.08t$	$2.90\ \mu$m $\sin 157.08t$	$-7.5036\ \mu$m $\sin 157.08t$
Third	$0.77\ \mu$m $\sin 157.08t$	$0.815\ \mu$m $\sin 157.08t$	$5.57\ \mu$m $\sin 157.08t$
Superposition of all modes	$-1.05\ \mu$m $\sin 157.08t$	$-18.46\ \mu$m $\sin 157.08t$	$-41.5\ \mu$m $\sin 157.08t$

Table 4: Transverse displacement $w(y,t)$ at various shaft positions

Mode	**At one-third of the shaft** ($y = L/3$)	**At two-thirds of the shaft** ($y = 2L/3$)	**At the end of the shaft** ($y = L$)
First	$-7.01\ \mu$m $\cos 157.08t$	$-22.62\ \mu$m $\cos 157.08t$	$-39.597\ \mu$m $\cos 157.08t$
Second	$5.18\ \mu$m $\cos 157.08t$	$2.90\ \mu$m $\cos 157.08t$	$-7.5036\ \mu$m $\cos 157.08t$
Third	$0.77\ \mu$m $\cos 157.08t$	$0.815\ \mu$m $\cos 157.08t$	$5.57\ \mu$m $\cos 157.08t$
Superposition of all modes	$-1.05\ \mu$m $\cos 157.08t$	$-18.46\ \mu$m $\cos 157.08t$	$-41.5\ \mu$m $\cos 157.08t$

be a point mass with rigid characteristics placed at the one-third and two-thirds end of the shaft, as shown in Figure 7.

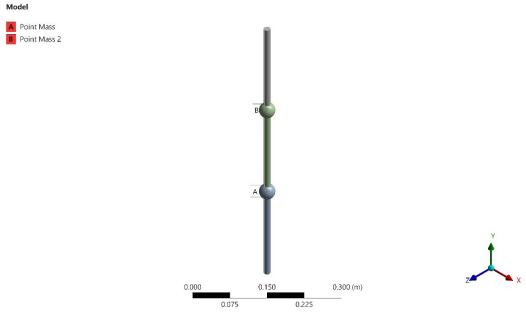

Figure 7: Geometric modelling of shaft with disc assumed as a point mass

4.2.2. *Meshing of model*

The model was meshed using body sizing with an element size of 0.0025m, as shown in Figure 8.

4.2.3. *Boundary condition and rotating force*

For performing harmonic response analysis of a two-disc cantilever shaft system in ANSYS, the system consists of a shaft with two point masses, labeled as A and B. A represents the first disc positioned at one-third of the length of the shaft while B represents the second disc positioned at two-thirds end of the shaft. A rotating force (D) with a magnitude of 1.0×10^{-4}kg m is applied at point A, introducing an unbalanced excitation to the system. The current analysis is set at 0 Hz, indicating

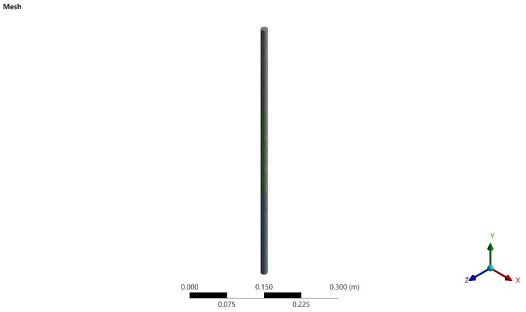

Figure 8: Meshing of the model

that no dynamic excitation is being applied yet, which suggests that the system is in a static or initial setup phase before running a frequency sweep. The setup is shown in Figure 9.

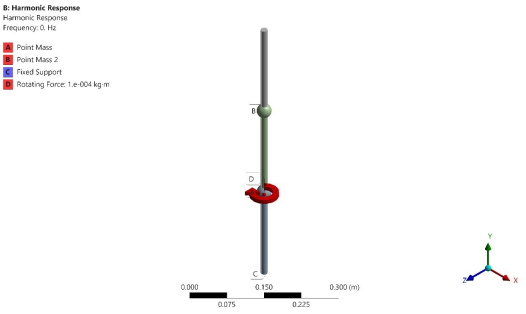

Figure 9: Boundary condition and rotating force

4.2.4. *Displacement results*

Applying the boundary conditions, the frequency response was found at the different positions of the shaft.

The amplitude at the end of the shaft (y=L) on both the horizontal and vertical planes was found to be 43.6 micrometers at 25 Hz, as shown in Figures 10 and 11, respectively.

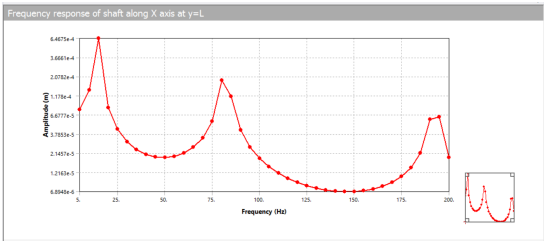

Figure 10: Frequency response at y=L in horizontal plane

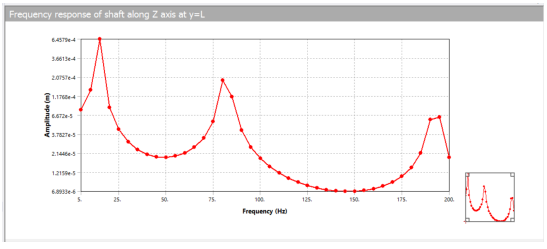

Figure 11: Frequency response at y=L in horizontal plane

Also, the amplitude was calculated at two-thirds of end of shaft (y=2L/3), and the amplitude was found to be 20.3 micrometers on both the horizontal and vertical planes as shown in figure as shown in Figure 12 and 13 respectively.

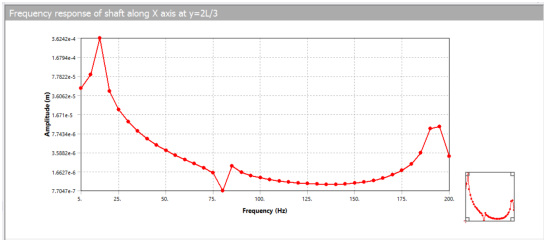

Figure 12: Frequency response at y=2L/3 in horizontal plane

4.3. Comparison of analytical and ANSYS

The amplitude found from Analytical and ANSYS are tabulated in Table 5.

From the above table, it is observed that the analytical results closely approximate the ANSYS result.

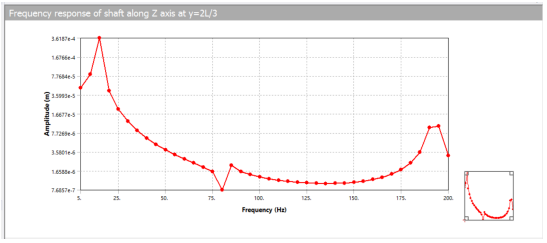

Figure 13: Frequency response at y=2L/3 in horizontal plane

5. Conclusion and reccomendations

This study analyzed the forced vibration response of a multi-disc shaft system with rotating unbalance, combining analytical modeling and finite element simulations using ANSYS. The shaft was modeled as a flexible Euler-Bernoulli beam incorporating gyroscopic effects, while the discs were treated as rigid bodies with unbalance. The equations of motion were derived using the extended Hamilton's principle and solved to obtain the system's dynamic response.

The result indicates that taking higher modes improves the accuracy of the result. For a shaft rotating at the speed of 1500 RPM, the transverse displacement at the free end of the shaft was found to be 41.5 micrometers on both the horizontal and vertical planes. The amplitude of vibration at the two-third of the length of the shaft is 18.46 micrometers analytically. The ANSYS result closely matches the analytical result.

The incorporation of material damping and higher modes of vibration while maintaining computational feasibility can result in better accuracy of the result. Further research may involve the study of nonlinear effects. In addition, damping devices such as magnetic, piezoelectric, or viscoelastic dampers may be optimized to enhance vibration control of high-speed rotation systems. Finally, the integration of machine learning (ML) and real-time condition monitoring for vibration analysis can advance more efficient fault detection and predictive maintenance strategies.

Funding

This research did not receive any specific grant from funding agencies in the public, commercial, or not-for-profit sectors.

Table 5: Comparison of Analytical and ANSYS results

S.N	Position on the shaft	Amplitude on Horizontal Plane			Amplitude on Vertical Plane		
		Analytical	ANSYS	Error (%)	Analytical	ANSYS	Error (%)
1	At position $y = L$ (end of shaft)	41.5 μm	43.6 μm	5.06%	41.5 μm	43.6 μm	5.06%
2	At position $y = 2L/3$ of the shaft	18.46 μm	20.3 μm	9.967%	18.46 μm	20.3 μm	9.967%

References

[1] Paulo P V D L. A time-domain methodology for rotor dynamics: analysis and force identification[D]. Portugal: Universidade Técnica de Lisboa, 2011.

[2] Bhatta N, Luintel M C, Tharu J K, et al. Vibration response of pelton turbine unit under rotating unbalance[C]// Proceedings of IOE Graduate Conference: volume 6. 2019: 101-107.

[3] Geradin M, Kill N. A new approach to finite element modelling of flexible rotors[J]. Engineering Computations, 1984, 1(1): 52-64.

[4] Shaw J, Shaw S W. Non-linear resonance of an unbalanced rotating shaft with internal damping[J]. Journal of Sound and Vibration, 1991, 147(3): 435-451.

[5] Hosseini S A A, Khadem S E. Analytical solution for primary resonances of a rotating shaft with stretching non-linearity[J]. Proceedings of the Institution of Mechanical Engineers, Part C: Journal of Mechanical Engineering Science, 2008, 222(9): 1655-1664.

[6] Luintel M C. Dynamic response of continuous shafts with different end conditions[J]. Journal of Innovations in Engineering Education, 2019, 2(1).

[7] Luintel M C. Development of polynomial mode shape functions for continuous shafts with different end conditions[J]. Journal of the Institute of Engineering, 2021, 16(1): 151-161.

[8] Ojha K, Luintel M C. Free vibration analysis of multidisc cantilever shaft system[C]// IOE Graduate Conference. 2023.

[9] Pradhan S, Luintel M C. Modal analysis of multi-disk rotor system[J]. Journal of Innovations in Engineering Education, 2024, 7(1): 38-44.

[10] Ameen Y M, Ali J K. Theoretical and experimental modal analysis of circular cross-section shaft[C]// IOP Conference Series: Materials Science and Engineering: volume 745. 2020: 012066.

[11] Saleem M A, Diwakar G, Satyanarayana M R S. Detection of unbalance in rotating machines using shaft deflection measurement during its operation[J]. IOSR Journal of Mechanical and Civil Engineering, 2012, 3(3): 8-20.

[12] Kumar B K, Diwakar G, Satyanarayana M R S. Determination of unbalance in rotating machine using vibration signature analysis[J]. International Journal of Modern Engineering Research, 2012, 2(5): 33415-33421.

[13] Chaphalkar S P, Khetre S N, Meshram A M. Modal analysis of cantilever beam structure using finite element analysis and experimental analysis[J]. American Journal of Engineering Research, 2015, 4(10): 178-185.

[14] Miranda W M, Faria M T C. Finite element method applied to the eigenvalue analysis of flexible rotors supported by journal bearings[J]. Engineering, 2014, 6(3): 127-137.

[15] Chhantyal B, Adhikari M, Chaudhary B B, et al. Use of polynomial mode shape function in free vibration analysis of cantilever pelton turbine[J]. Kathford Journal of Engineering and Management, 2025, 4(1): 92-101.